FSD: Frequency Space Differential measurement of CMB spectral distortions

Suvodip Mukherjee, Joseph Silk, Benjamin D. Wandelt

Monthly Notices
of the
ROYAL ASTRONOMICAL SOCIETY

MNRAS **477,** 4473–4482 (2018)
Advance Access publication 2018 April 7

doi:10.1093/mnras/sty888

FSD: Frequency Space Differential measurement of CMB spectral distortions

Suvodip Mukherjee,[1,2,3]★ Joseph Silk[2,3,4,5] and Benjamin D. Wandelt[1,2,3,6]

[1]*Center for Computational Astrophysics, Flatiron Institute, 162 5th Avenue, New York, NY 10010, USA*
[2]*Institut d'Astrophysique de Paris, 98 bis Boulevard Arago, F-75014 Paris, France*
[3]*Sorbonne Universités, Institut Lagrange de Paris, 98 bis Boulevard Arago, F-75014 Paris, France*
[4]*Department of Physics & Astronomy, Bloomberg Center for Physics and Astronomy, The Johns Hopkins University, Room 366, 3400 N. Charles Str, Baltimore, MD 21218, USA*
[5]*Beecroft Institute for Cosmology and Particle Astrophysics, University of Oxford, Keble Road, Oxford OX1 3RH, UK*
[6]*Departments of Physics and Astronomy, University of Illinois at Urbana-Champaign, 1002 W Green St, Urbana, IL 61801, USA*

Accepted 2018 April 5. Received 2018 March 11; in original form 2018 January 29

ABSTRACT

Although the cosmic microwave background (CMB) agrees with a perfect blackbody spectrum within the current experimental limits, it is expected to exhibit certain spectral distortions with known spectral properties. We propose a new method Frequency Space Differential (FSD) to measure the spectral distortions in the CMB spectrum by using the inter-frequency differences of the brightness temperature. The difference between the observed CMB temperature at different frequencies must agree with the frequency derivative of the blackbody spectrum in the absence of any distortion. However, in the presence of spectral distortions, the measured inter-frequency differences would also exhibit deviations from blackbody that can be modelled for known sources of spectral distortions like y and μ. Our technique uses FSD information for the CMB blackbody, y, μ, or any other sources of spectral distortions to model the observed signal. Successful application of this method in future CMB missions can provide an alternative method to extract spectral distortion signals and can potentially make it feasible to measure spectral distortions without an internal blackbody calibrator.

Key words: cosmic background radiation – cosmology: observations.

1 INTRODUCTION

Imprints of spectral distortions in the cosmic microwave background (CMB) are a prediction of the Standard Cosmological Model (Zeldovich & Sunyaev 1969; Chluba, Khatri & Sunyaev 2012; Chluba & Sunyaev 2012a; Khatri & Sunyaev 2012a,b; Khatri, Sunyaev & Chluba 2012; Emami et al. 2015; Hill et al. 2015; Chluba 2016). Measurement of signals such as y and μ distortions will help to validate our standard cosmological model. Indeed the essential ansatz of structure formation by gravitational instability predicts weak but potentially measurable μ distortions (Sunyaev & Zeldovich 1970; Hu, Scott & Silk 1994; Chluba et al. 2012; Khatri et al. 2012; Pajer & Zaldarriaga 2012). Discoveries of any other kinds of spectral distortions can open up a window to new physics. One of the main goals of several next-generation cosmology missions is to measure the spectral distortions in the CMB blackbody spectrum. The first observational bound on the spectral distortion was given by Far Infrared Absolute Spectrophotometer (FIRAS; Smoot et al. 1991; Mather et al. 1994; Fixsen et al. 1997) with $\mu < 9 \times 10^{-5}$ and $y < 15 \times 10^{-6}$ at 95 per cent C.L. FIRAS used an absolute blackbody internal calibrator to measure the monopole of the CMB temperature field and constrained its temperature $T = 2.725 \pm 0.001$ K (Mather et al. 1999; Fixsen 2009). With the recent CMB anisotropy data, measurements of Sunyaev–Zel'dovich (SZ) clusters (Staniszewski et al. 2009; Hasselfield et al. 2013; Bleem et al. 2015; Planck Collaboration XXVII 2016) and bounds on the fluctuating y and μ have also been obtained (Khatri & Sunyaev 2015a,b).

Several concepts are under discussion for a post-Planck CMB polarization mission in space, including spectrometry [PIXIE (Kogut et al. 2011) or PRISM (André et al. 2014)], high-resolution imaging (CMBPOL) (Dunkley et al. 2009), or a mission with modest resolution focusing on the large-angle primordial anisotropy (LiteBIRD) (Matsumura et al. 2016). While imaging and spectroscopy are often presented as mutually exclusive concepts we propose a hybrid approach to image spectral distortions which we term the Frequency Space Differential (FSD) method. This technique uses a differential measurement of the CMB between different frequencies and therefore does not require an absolute calibrator.

★ E-mail: smukherjee@flatironinstitute.org (SM);
joseph.silk@physics.ox.ac.uk (JS); bwandelt@iap.fr (BDW)

In this paper, we propose a new technique for measuring the spectral distortions in the CMB that can avoid using an absolute blackbody calibrator. We describe the possibility of measuring the spectral distortion in CMB by measuring the inter-frequency differences of the sky intensity and matching it with the theoretical prediction of the signal frequency spectrum. The blackbody spectrum predicts a well-known intensity or brightness temperature at every frequency. As a result, the difference of the blackbody intensity between two different frequencies can predict a unique spectral shape, and we can obtain an all-sky FSD map of the blackbody spectrum. In the presence of any spectral distortions in the blackbody intensity, the derivative of the observed intensity is a composite signature of frequency derivatives of the blackbody spectrum and other sources of spectral distortions.

We will see that the key idea is to design the measurement such that any gain fluctuations couple only to the frequency derivative of the blackbody spectrum rather than the blackbody spectrum itself. A similar approach was discussed recently by Sironi (2017) who also proposed a detector design. The idea of differential measurement in the frequency domain was also discussed earlier in the context of recombination line (Sunyaev & Chluba 2009; Sathyanarayana Rao et al. 2015).

Even in the absence of an absolute calibrator, an overall calibration can be obtained from the time-dependent velocity dipole due to the orbital motion around the Sun. This effect can be extracted from a multiyear campaign due to its annual modulation. Its frequency spectrum only depends on well-known relativistic effects and is directly proportional to the derivative of the blackbody spectrum. It can therefore serve as an absolute and robust calibrator for the FSD technique. This effect was used in Fixsen (2009) to recalibrate the FIRAS data using the *WMAP* time ordered data.

In this paper, we discuss the main idea of using the frequency derivative of the spectral distortion signal to measure the μ and y distortions without an absolute calibrator (in an analogous way to how *WMAP* created a map from a purely differential measurement of the anisotropies, in contrast to *Planck* that used an internal reference). We prescribe possible measurement strategies and statistical techniques to implement this method for future CMB missions. The implementation of this method to a particular mission puts requirements on measurement technique, scan strategy, detector properties, and calibration techniques.

This paper is organized as follows. Section 2 sets out the form of the expected signals in the sky when observed differentially in frequency space. In Section 3, we discuss how to form differential combinations of nearby frequency channels such that inter-channel calibration errors do not couple to the CMB monopole but only to the derivative of the *Planck* spectrum. Once this major source of noise is removed, the remaining signal needs to be cleaned from foreground contamination. A method for removal of those contaminants and recovery of the spectral distortion signal is given in Section 4. In Section 5, we discuss the main requirements our approach places on instrument design. In Section 6, we outline the necessary steps to implement FSD method. We conclude in Section 7.

2 FORMALISM

The all-sky average temperature field of the CMB exhibits a blackbody spectrum ($S_{\rm brightness} \equiv c^2 B_\nu / 2k_{\rm B}\nu^2 = h\nu/k_{\rm B}(e^{h\nu/k_{\rm B}T_{\rm CMB}}-1)$) with a brightness temperature $S_{\rm brightness} = 2.7255\,{\rm K}$ in the RJ limit ($h\nu/k_{\rm B}T_{\rm CMB} < 1$). Any deviation from the blackbody spectrum can be parametrized as (Mather et al. 1994; Fixsen et al. 1997)

$$I_\nu^o = B_\nu(T_{\rm CMB}) + \Delta T_{\rm CMB}\frac{\partial B}{\partial T} + \Delta I_\nu^{\rm gal} + u\frac{\partial B}{\partial u}, \tag{1}$$

where I_ν^o is the observed intensity in the sky and the first and second terms are the blackbody spectrum and fluctuations in the blackbody due to CMB temperature fluctuations. The third term indicates the galactic contamination and the last term is the spectral distortion due to cosmological processes (like $u \equiv \mu,\ y$). The observed intensity of the sky at every frequency should be compared with an internal blackbody calibrator fixed at a particular temperature to deduce the temperature of the CMB field and also any departure from blackbody. The FIRAS (Mather et al. 1994; Fixsen et al. 1997) experiment used an internal blackbody calibrator to measure the CMB temperature field and also provided the first observational constraints on $\mu,\ y$ distortions as 9×10^{-5} and 15×10^{-6} at 95 per cent C.L., respectively. Measurement of any well-motivated CMB spectral distortions to values of cosmological interest (Zeldovich & Sunyaev 1969; Hu et al. 1994; Sunyaev & Chluba 2009; Chluba 2010; Chluba & Sunyaev 2012a,b; Chluba et al. 2012; Khatri & Sunyaev 2012a,b; Khatri et al. 2012; Balashev et al. 2015; Emami et al. 2015; Hill et al. 2015; Kholupenko et al. 2015; Chluba 2016) requires a much better absolute blackbody calibrator than FIRAS.

We will show how to estimate cosmological spectral distortions with any given spectrum using the FSD technique. Astrophysical sources add contaminations with approximately known spectra. We will find that these have a similar effect on the FSD technique as on absolutely calibrated spectral distortion measurements.

2.1 Probing spectral distortions through spectral derivatives

The observed CMB blackbody intensity, along with spectral distortions like y and μ, also gets contaminated by several galactic astrophysical emissions in the CMB frequency range by processes like synchrotron, free–free, spinning dust, thermal dust, etc. The total emission can be written in terms of intensity at a particular frequency ν in a particular pixel ($\hat{p}$) as a superimposition of various effects that can be written in the form

$$\begin{aligned} I_\nu(\hat{p}) =& \bar{I}(I_\nu^{\rm pl} + \Delta T_{\rm CMB}(\hat{p})I_\nu^T + \mu(\hat{p})I_\nu^\mu + y(\hat{p})I_\nu^y) \\ &+ A_{\rm dust}(\hat{p})I_\nu^{\rm dust} + A_{\rm syn}(\hat{p})I_\nu^{\rm syn} + A_{\rm free}(\hat{p})I_\nu^{\rm free} \\ &+ A_{\text{spin-dust}}(\hat{p})I_\nu^{\text{spin-dust}}, \end{aligned} \tag{2}$$

where $x = h\nu/k_{\rm B}T_{\rm CMB} = \nu/\nu_{\rm CMB}$, $\bar{I} = 2k_{\rm B}^3T_{\rm CMB}^3/c^2h^2$, and A_j are dimensionless and defined in units of current *Planck* measurements (Planck Collaboration X 2016) (denoted by $\bar{A}_j$). In terms of the brightness temperature, we can write this as

$$\begin{aligned} S_\nu(\hat{p}) =& \frac{c^2}{2k_{\rm B}\nu^2}I_\nu(\hat{p}) \\ S_\nu(\hat{p}) =& K_\nu^{\rm pl} + A_{\rm CMB}(\hat{p})K_\nu^T + A_\mu(\hat{p})K_\nu^\mu + A_y(\hat{p})K_\nu^y \\ &+ A_{\rm dust}(\hat{p})K_\nu^{\rm dust} + A_{\rm syn}(\hat{p})K_\nu^{\rm syn} + A_{\rm free}(\hat{p})K_\nu^{\rm free} \\ &+ A_{\text{spin-dust}}(\hat{p})K_\nu^{\text{spin-dust}}, \end{aligned} \tag{3}$$

where we defined $K_\nu^j = I_\nu^j/\nu^2$. The spectral shape of the intensity for different components (depicted in Fig. 1) can be written as

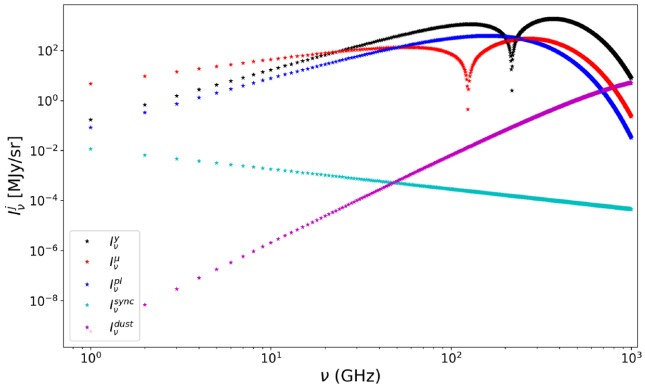

Figure 1. We plot the intensity spectrum for different sources of spectral distortions for y distortions (black), μ distortions (red), and blackbody spectrum (blue) at $T_0 = 2.7255$ K. We also plot the two sources of foreground contaminations, synchrotron (cyan), and dust (magenta). The synchrotron spectrum is plotted without the external templates.

$$
\begin{aligned}
I_\nu^{\rm pl} &= \frac{x^2 x}{(e^x-1)}, {}^T_\nu = \frac{x^4 e^x}{(e^x-1)^2}, \\
I_\nu^{\mu} &= \frac{x^3 e^x}{(e^x-1)^2}\left(\frac{x}{2.1923}-1\right), \\
I_\nu^{y} &= \frac{x^4 e^x}{(e^x-1)^2}\left(x\left(\frac{e^x+1}{e^x-1}\right)-4\right), \\
I_\nu^{\rm dust} &= \bar{A}_{\rm dust}\left(\frac{\nu}{\nu_0}\right)^{\beta_d+3}\left(\frac{e^{\gamma\nu_0}-1}{e^{\gamma\nu}-1}\right), \\
\gamma &= \frac{h}{k_b T_d},\ T_d = 18\,{\rm K},\ \nu_0 = 545\,{\rm GHz},\ \beta_d = 1.55, \\
I_\nu^{\rm syn} &= \bar{A}_{\rm syn}\left(\frac{\nu_0}{\nu}\right)^{\alpha_s}\frac{f_s(\nu/\alpha)}{f_s(\nu_0/\alpha)} \\
\nu_0 &= 408\,{\rm MHz},\ f_s = {\rm templates},\ \alpha_s = 0.8, \\
I_\nu^{\rm free} &= \bar{A}_{\rm free}\nu^2 T_{\rm e}(1-e^{-\tau}), \\
\tau &= 0.05468 T_{\rm e}^{-3/2}\nu_9^{-2}\log(e^{[5.96-\sqrt{3}\pi\log(\nu_9 T_4^{-3/2})]}+e), \\
\nu_9 &= \frac{\nu}{\rm GHz},\ T_4 = T_{\rm e}/10^4, \\
I_\nu^{\rm spin\text{-}dust} &= \bar{A}_{\rm spin\text{-}dust}\frac{f_{\rm sd}(\nu\nu_{p0}/\nu_p)}{f_{\rm sd}(\nu_0\nu_{p0}/\nu_p)} \\
\nu_{p0} &= 30\,{\rm GHz},\ f_{\rm sd} = {\rm templates}.
\end{aligned}
\tag{4}
$$

The all-sky average measurement of equation (2) obtains the contribution only from the monopole term, whereas the differential measurement of equation (2) between different pixels gets the contribution only from the fluctuation parts ($\Delta T_{\rm CMB}(\hat{p})$, $\Delta\mu(\hat{p})$ and $\Delta y(\hat{p})$), and captures no contributions from the monopole of the CMB or any other spectral distortion signals. However, the differential measurement in frequency space for sky brightness temperature ($\mathcal{S}_{\nu_{ji}} = S_{\nu_j} - S_{\nu_i}$) and intensity ($\mathcal{I}_{\nu_{ji}} = I_{\nu_j} - I_{\nu_i}$) has non-zero contributions both from the monopole and from the fluctuation part, which can be written as

$$
\begin{aligned}
\mathcal{I}_{\nu_{ji}}(\hat{p}) = \Bigg(& \mathcal{F}^{\rm pl}_{\nu_{ji}} + \Delta I_{\rm CMB}(\hat{p})\mathcal{F}^{T}_{\nu_{ji}} + \mu(\hat{p})\mathcal{F}^{\mu}_{\nu_{ji}} + y(\hat{p})\mathcal{F}^{y}_{\nu_{ji}} \\
& + A_{\rm dust}\mathcal{F}^{\rm dust}_{\nu_{ji}}(\hat{p}) + A_{\rm syn}\mathcal{F}^{\rm syn}_{\nu_{ji}}(\hat{p}) + A_{\rm free}\mathcal{F}^{\rm free}_{\nu_{ji}}(\hat{p}) \\
& + A_{\rm spin\text{-}dust}\mathcal{F}^{\rm spin\text{-}dust}_{\nu_{ji}}(\hat{p})\Bigg)\Delta\nu_{ji},
\end{aligned}
\tag{5}
$$

$$
\begin{aligned}
\mathcal{S}_{\nu_{ji}}(\hat{p}) = \Bigg(& \mathcal{D}^{\rm pl}_{\nu_{ji}} + A_{\rm CMB}(\hat{p})\mathcal{D}^{T}_{\nu_{ji}} + A_{\mu}(\hat{p})\mathcal{D}^{\mu}_{\nu_{ji}} \\
& + A_{y}(\hat{p})\mathcal{D}^{y}_{\nu_{ji}} + A_{\rm dust}(\hat{p})\mathcal{D}^{\rm dust}_{\nu_{ji}} + A_{\rm syn}(\hat{p})\mathcal{D}^{\rm syn}_{\nu_{ji}} \\
& + A_{\rm free}(\hat{p})\mathcal{D}^{\rm free}_{\nu_{ji}} + A_{\rm spin\text{-}dust}(\hat{p})\mathcal{D}^{\rm spin\text{-}dust}_{\nu_{ji}}\Bigg)\Delta\nu_{ji}.
\end{aligned}
\tag{6}
$$

For closely spaced frequency channels, i.e. small $\Delta\nu_{ji} = \nu_j - \nu_i$ this can be related to the derivative of the theoretical frequency spectrum $\mathcal{D}^x_{\nu_{ji}}(\hat{p}) = \partial S^x/\partial\nu|_{\nu_{ji}}$ and $\mathcal{F}^x_{\nu_{ji}}(\hat{p}) = \partial I^x/\partial\nu|_{\nu_{ji}}$ evaluated at the mid-point $\nu_{ji} = (\nu_j + \nu_i)/2$. The theoretical FSD spectrum of the various sources can be expressed in terms as

$$
\begin{aligned}
\mathcal{F}^{\rm pl}_{\nu} &= \frac{\bar{I}}{\nu_{\rm CMB}}\frac{x^2}{(e^x-1)}\left[3-\frac{xe^x}{(e^x-1)}\right], \\
\mathcal{F}^{T}_{\nu} &= \frac{\bar{I}}{\nu_{\rm CMB}}\frac{x^4 e^x}{(e^x-1)^2}\left[\frac{4}{x}+1-\frac{2e^x}{(e^x-1)}\right], \\
\mathcal{F}^{\mu}_{\nu} &= \frac{\bar{I}}{\nu_{\rm CMB}}\left[\frac{x^2e^x}{(e^x-1)^2}\left[3+x-\frac{2xe^x}{(e^x-1)}\right]\left[\frac{x}{2.19}-1\right]\right. \\
&\quad \left.+\frac{x^3e^x}{2.19(e^x-1)^2}\right], \\
\mathcal{F}^{y}_{\nu} &= \frac{\bar{I}}{\nu_{\rm CMB}}\left[\frac{I^y_\nu}{x}\left(4+x-\frac{2xe^x}{(e^x-1)}\right)\right. \\
&\quad \left.+\frac{x^4e^x}{(e^x-1)^2}\left(\left(\frac{e^x+1}{e^x-1}\right)+\left(\frac{xe^x}{e^x-1}\right)-\left(\frac{xe^x(e^x+1)}{(e^x-1)^2}\right)\right)\right], \\
\mathcal{F}^{\rm dust}_{\nu} &= \bar{I}_{\rm dust}\left(\frac{\nu}{\nu_0}\right)^{\beta_d+3}\left(\frac{e^{\nu_0/T_d}-1}{e^{\nu/T_d}-1}\right)\left[\frac{\beta_d+3}{\nu}-\frac{\gamma e^{\gamma\nu}}{(e^{\gamma\nu}-1)}\right], \\
\mathcal{F}^{\rm syn}_{\nu} &= \bar{I}_{\rm sync}\left(\frac{\nu_0}{\nu}\right)^{\alpha_s}\left(\frac{-\alpha_s}{\nu}\frac{f_s(\nu/\alpha)}{f_s(\nu_0/\alpha)}+\frac{\partial f_s(\nu/\alpha)}{\partial\nu}\frac{1}{f_s(\nu_0/\alpha)}\right), \\
\mathcal{F}^{\rm free}_{\nu} &= (\bar{I}_{\rm free})T_{\rm e}(2\nu(1-e^{-\tau})+\nu^2 e^{\tau}\frac{\partial\tau}{\partial\nu}), \\
\mathcal{F}^{\rm spin\text{-}dust}_{\nu} &= (\bar{I}_{\rm spin\text{-}dust})\left(\frac{\nu_0}{\nu}\right)^2\left(\frac{-2}{\nu}\frac{f_{\rm sd}(\nu\nu_{p0}/\nu_p)}{f_{\rm sd}(\nu_0\nu_{p0}/\nu_p)}\right. \\
&\quad \left.+\frac{\partial f_{\rm sd}(\nu\nu_{p0}/\nu_p)}{\partial\nu}\frac{1}{f_{\rm sd}(\nu_0\nu_{p0}/\nu_p)}\right),
\end{aligned}
\tag{7}
$$

$$
\begin{aligned}
\mathcal{D}^{\rm pl}_{\nu} &= \frac{A_{\rm CMB}}{\nu_{\rm CMB}}\frac{1}{(e^x-1)}\left[1-\frac{xe^x}{(e^x-1)}\right], \\
\mathcal{D}^{T}_{\nu} &= \frac{1}{\nu_{\rm CMB}}\frac{x^2e^x}{(e^x-1)^2}\left[\frac{2}{x}+1-\frac{2e^x}{(e^x-1)}\right], \\
\mathcal{D}^{\mu}_{\nu} &= \frac{T_{\rm CMB}}{\nu_{\rm CMB}}\frac{e^x}{(e^x-1)^2}\left[-1-x+\frac{2xe^x}{(e^x-1)}\right]\left[\frac{x}{2.19}-1\right] \\
&\quad +\frac{xe^x}{2.19(e^x-1)^2}, \\
\mathcal{D}^{y}_{\nu} &= \frac{T_{\rm CMB}}{\nu_{\rm CMB}}\left[\Delta n^y_\nu\left(2+x-\frac{2xe^x}{(e^x-1)}\right)\right. \\
&\quad \left.+\frac{x^2e^x}{(e^x-1)^2}\left(\left(\frac{e^x+1}{e^x-1}\right)+\left(\frac{xe^x}{e^x-1}\right)-\left(\frac{xe^x(e^x+1)}{(e^x-1)^2}\right)\right)\right], \\
\mathcal{D}^{\rm dust}_{\nu} &= \bar{A}_{\rm dust}\left(\frac{\nu}{\nu_0}\right)^{\beta_d+1}\left(\frac{e^{\nu_0/T_d}-1}{e^{\nu/T_d}-1}\right)\left[\frac{\beta_d+1}{\nu}-\frac{\gamma e^{\gamma\nu}}{(e^{\gamma\nu}-1)}\right], \\
\mathcal{D}^{\rm syn}_{\nu} &= \bar{A}_{\rm syn}\left(\frac{\nu_0}{\nu}\right)^2\left(\frac{-2}{\nu}\frac{f_s(\nu/\alpha)}{f_s(\nu_0/\alpha)}+\frac{\partial f_s(\nu/\alpha)}{\partial\nu}\frac{1}{f_s(\nu_0/\alpha)}\right), \\
\mathcal{D}^{\rm free}_{\nu} &= \bar{A}_{\rm free}T_{\rm e}e^{\tau}\frac{\partial\tau}{\partial\nu}, \\
\mathcal{D}^{\rm spin\text{-}dust}_{\nu} &= \bar{A}_{\rm spin\text{-}dust}\left(\frac{\nu_0}{\nu}\right)^2\left(\frac{-2}{\nu}\frac{f_{\rm sd}(\nu\nu_{p0}/\nu_p)}{f_{\rm sd}(\nu_0\nu_{p0}/\nu_p)}\right. \\
&\quad \left.+\frac{\partial f_{\rm sd}(\nu\nu_{p0}/\nu_p)}{\partial\nu}\frac{1}{f_{\rm sd}(\nu_0\nu_{p0}/\nu_p)}\right),
\end{aligned}
\tag{8}
$$

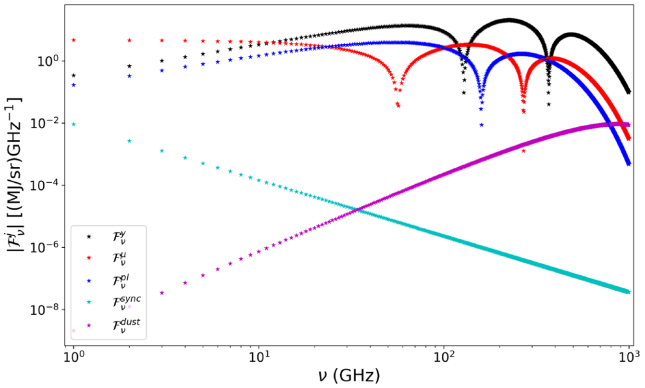

Figure 2. The FSD spectra in terms of intensities of the y distortions (black), μ distortions (red), blackbody spectrum (blue), synchrotron (cyan), and dust (magenta) are depicted over a wide frequency range that is usually accessible by CMB missions. The synchrotron spectrum is plotted without the external templates.

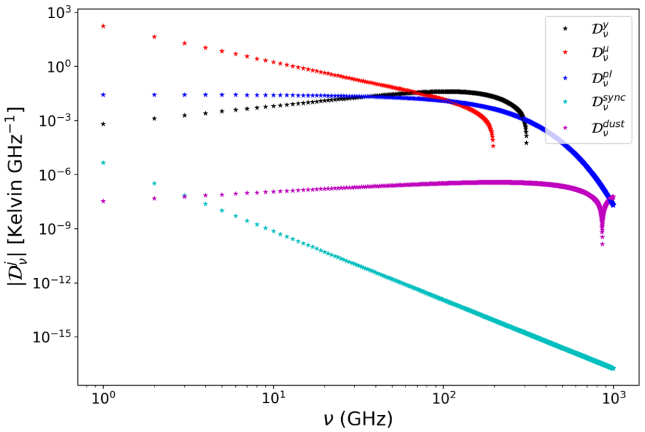

Figure 3. The FSD spectra of the y distortions (black), μ distortions (red), and blackbody spectrum (blue) along with foregrounds like synchrotron (cyan) and dust (magenta) are depicted over a wide frequency range that is usually accessible by CMB missions. The synchrotron spectrum is plotted without the external templates.

where $\Delta n_\nu^y = K_\nu^y / x T_{\rm CMB}$ and $\bar{A}_j$ are the amplitude of the signal as measured by *Planck* measurements (Planck Collaboration X 2016). Equation (6) can be written in matrix notation as

$$\mathcal{S}(\hat{p}) = \mathbf{DA}(\hat{p}). \tag{9}$$

Here, $\mathbf{D}$ is the matrix of the FSD spectrum with components $\mathcal{D}_{ji} = \mathcal{D}^j_{\nu_i} \Delta\nu_i$ and $\mathbf{A}$ is the column matrix composed of the signals. This equation relates the FSD with the known theoretical spectrum of several sources. The FSD spectrum for intensity and brightness temperature for different sources are plotted in Figs 2 and 3, respectively. As is clear from Fig. 3, the spectrum for each of the sources is distinct. For μ distortions, the FSD signal is mainly strong at low frequencies and decays rapidly. The y distortions peak at higher frequencies with a much wider FSD spectrum ($\nu \in 40{-}300$ GHz) than μ. A mission to constrain both y and μ therefore requires a combination of low- and high-frequency channels. We will leave a detailed design study of an optimal distribution of channel frequencies and bandwidths to future work. An estimator such as modified internal linear combination (MILC; Hurier, Macías-Pérez & Hildebrandt 2013) combines all frequency channels to reject foreground contamination and improve signal-to-noise ratio (SNR). We will develop the formalism of such an estimator in the context of the FSD technique in Section 4.

In the next section, we describe the dominant source of systematic error in this method and how to mitigate it.

3 MEASUREMENT TECHNIQUE AND SYSTEMATIC ERRORS

Usage of the FSD technique to measure CMB spectral distortions is only possible if the temperature differences between frequency channels can be determined with sufficient systematic error control. Though the measurement techniques and detector properties depend on specific missions, we discuss the basic requirements that should be addressed in order to use the FSD method in this section.

CMB experiments for the last three decades have used several detector technologies like directly coupled bolometers, antenna coupled bolometers, MKIDS etc. In this section, we mainly focus on the bolometer-like detectors. However, this method can also be applied to other techniques.

For bolometer-like detectors, the power measured from a blackbody source can be written as (Richards 1994)

$$P_\nu = \int_0^\infty {\rm d}\nu\, w(\nu) \frac{2h\nu^3}{c^2(\exp(x)-1)} A\Omega, \tag{10}$$

where $x = h\nu/k_{\rm B}T$, $w(\nu)$ is the transmission function and $A\Omega$ is the throughput or *etendue*, which is equal to $\lambda^2 = (c/\nu)^2$ for a diffraction limited beam experiment (Richards 1994). As a result, equation (10) becomes

$$\begin{aligned} P_\nu &= \int_0^\infty {\rm d}\nu\, w(\nu) \frac{2h\nu}{(\exp(x)-1)}, \\ P_\nu &= \int_0^\infty {\rm d}\nu\, w(\nu) 2k_{\rm B} S_\nu, \end{aligned} \tag{11}$$

where S_ν is the brightness temperature, which in the RJ limit reduces to (Richards 1994)

$$P_\nu = \int_0^\infty {\rm d}\nu\, w(\nu) 2k_{\rm B} T. \tag{12}$$

So the output voltage from a bolometer detector is directly related to the sky brightness temperature S_ν. In the next section, we will calculate the output voltage from bolometer-like systems and hence the corresponding output voltage V_ν at a frequency ν.

3.1 The non-differential technique of measuring the radiation field

To illustrate the problem, we will first discuss why non-differential methods will not be able to provide useful constraints on spectral distortions. The radiation impinging on a pixel ($\hat{p}$) at a frequency ν_i of the detector produces a voltage $V_{\nu_i}(\hat{p})$ that is related to the observed temperature field by the gain factor G_{ν_i} as

$$T_{\nu_i}(\hat{p}) = G_{\nu_i} V_{\nu_i}(\hat{p}) + T^{\rm off}_{\nu_i}, \tag{13}$$

where $T^{\rm off}_{\nu_i}$ is the instrumental off-set temperature. In the absence of mean detector noise, the measured temperature at a pixel $\hat{p}$ in frequency ν_i is related to the theoretical signal by the relation,

$$T_{\nu_i}(\hat{p}) = S_{\nu_i}(\hat{p}) + T^{\rm off}_{\nu_i}. \tag{14}$$

However, detectors even with a known and stable gain factor G_{ν_i} and offset temperature $T^{\rm off}_{\nu_i} = 0$ exhibit variations δG_{ν_i} and $\delta T^{\rm off}_{\nu_i}$ that are the sources of systematic errors that propagate through the measurements. As a result, the systematic error associated with the

temperature field (equation 13) are due to the gain and off-set error, which can be written as

$$(\sigma_{\nu_i})^2_{\rm sys} \equiv (\delta T_{\nu_i}(\hat{p}))^2 = \left(\frac{\delta G_{\nu_i}}{G_{\nu_i}}\right)^2 (G_{\nu_i} V_{\nu_i}(\hat{p}))^2 + (\delta T^{\rm off}_{\nu_i})^2. \quad (15)$$

After using equation (14), above equation can be expressed as

$$(\sigma_{\nu_i})^2_{\rm sys} = \left(\frac{\delta G_{\nu_i}}{G_{\nu_i}}\right)^2 (S_{\nu_i}(\hat{p}))^2 + (\delta T^{\rm off}_{\nu_i})^2. \quad (16)$$

The dominant contribution to $S_{\nu_i}(\hat{p})$ is the blackbody temperature field of CMB ($K^{pl}_{\nu_i}$ in equation 2). As a result, the dominant source of systematic error in equation (16) is induced by the coupling between gain error δG_{ν_i} and $K^{\rm pl}_{\nu_i}$. For the typical values of gain error (of order 0.1–0.01 per cent),[1] the contribution of the systematic error is greater than the usual signal strength of μ and y distortions. So to measure the spectral distortion signals, an absolute internal blackbody calibrator with a precisely known reference temperature is required under this method of measurement.

In the following subsection, we will introduce a *new differential method* that can reduce the systematic error without an absolute calibrator and also use the cross-calibration between the frequency channels to minimize the budget of the systematic error.

3.2 The FSD technique for measuring the radiation field

The incoming electromagnetic waves (composed of multiple components) from the sky at a particular frequency channel ν_i falls on the detector (operating at this frequency) will have an induced voltage, which we define as V_{ν_i}. In the FSD technique, we propose the measurement of the difference in the amplitude of electromagnetic field at two different frequencies by taking the difference between the induced voltages ($V_{\nu_j} - V_{\nu_i}$). This differential measurement of the signal carries the information of the change in the electromagnetic field of CMB (and also in other contaminations) with variation in the frequency. The measured differential voltage can be converted into a temperature difference by a known gain factor G_{ν_i} and G_{ν_j} by the relation

$$\mathcal{T}_{\nu_{ji}}(\hat{p}) = G_{\nu_j}\delta V_{\nu_{ji}}(\hat{p}) + G_{\nu_i}\delta V_{\nu_{ji}}(\hat{p}), \quad (17)$$

where $\delta V_{\nu_{ji}}(\hat{p}) = (V_{\nu_j} - V_{\nu_i})/2$, $\nu_{ji} = (\nu_j + \nu_i)/2$, and the off-set temperature difference between the two channels is assumed to be zero. If $G_{\nu_i} = G_{\nu_j}$, then the above equation is directly related to the theoretical FSD signal $\mathcal{S}_{\nu_{ji}}$ (equation 6) as

$$\mathcal{T}_{\nu_{ji}}(\hat{p}) \equiv G_{\nu_j}(\delta V_{\nu_{ji}}(\hat{p}) + \delta V_{\nu_{ji}}(\hat{p})) = \mathcal{S}_{\nu_{ji}}(\hat{p}). \quad (18)$$

However, if $G_{\nu_i} = G_{\nu_j} + \Delta G_{\nu_{ji}}$, then

$$\mathcal{T}_{\nu_{ji}}(\hat{p}) = \mathcal{S}_{\nu_{ji}}(\hat{p}) + \frac{\Delta G}{G_{\nu_j}} G_{\nu_j}\delta V_{\nu_{ji}}(\hat{p}), \quad (19)$$

where the second term is an extra bias originating from the difference of the gain factors between two frequency channels. This indicates that any variation in gain factor will affect the measurement by coupling it with the difference in the voltages and not with the absolute value of the voltages. As the voltage difference between two channels have the dominant contribution from the FSD spectrum of the blackbody $\mathcal{S}^{pl}_{\nu_{ji}}$, along with other contaminations, the above equation can be written as

$$\mathcal{T}_{\nu_{ji}}(\hat{p}) \approx \mathcal{S}_{\nu_{ji}}(\hat{p}) + \frac{\Delta G}{G_{\nu_j}} \mathcal{S}_{\nu_{ji}}(\hat{p}). \quad (20)$$

[1] A detailed description of the systematic error is given in Section 3.4.

The variance of equation (17) only due to the uncorrelated systematic errors in the gain factor and off-set temperature can be written as

$$(\sigma^2_{\nu_{ji}})_{\rm sys} \equiv (\delta\mathcal{T}_{\nu_{ji}})^2 = \left(\frac{\delta G_{\nu_i}}{G_{\nu_i}}\right)^2 G^2_{\nu_i}\delta V^2_{\nu_{ji}} + \left(\frac{\delta G_{\nu_j}}{G_{\nu_j}}\right)^2 G^2_{\nu_j}\delta V^2_{\nu_{ji}} + (\delta T^{\rm off}_{\nu_j})^2 + (\delta T^{\rm off}_{\nu_i})^2. \quad (21)$$

Here, $(\delta T^{\rm off}_{\nu_i})^2$ denotes the variance in the offset measurement. The systematic error is related to the voltage difference which according to equation (19) have major contribution from the FSD spectrum of CMB blackbody along with the contributions from synchrotron at low frequency and dust at high frequency. The relative intensity of the CMB, synchrotron, and dust can be seen in Fig. 3. The comparison of equations (15) and (21) exhibits the key difference between the non-differential technique and the FSD technique. The systematic error is related to the absolute blackbody signal in the former case and to the difference of the sky temeperature in the latter case. As depicted in Fig. 3, for $\Delta\nu = 1$ GHz, the amplitude of FSD spectrum of blackbody is two orders of magnitude below the blackbody signal. Hence, the systematic error between these two methods will also differ by two orders of magnitude.

The total error due to both the systematic and statistical errors can be written as

$$(\sigma^2_{\nu_{ji}})_{\rm tot} = (\sigma^2_{\nu_{ji}})_{\rm sys} + (\sigma^2_{\nu_{ji}})_{\rm stat}, \quad (22)$$

where we define the statistical error in terms of the uncorrelated instrumental noise as

$$(\sigma^2_{\nu_{ji}})_{\rm stat}(\hat{p}) = (\delta T^N_{\nu_i}(\hat{p}))^2 + (\delta T^N_{\nu_j}(\hat{p}))^2. \quad (23)$$

The key concept of the FSD method that separates it from the usual absolute calibration method is the fact that FSD is not the difference of the already calibrated sky temperature, rather it is the calibration of the difference in the sky temperature.

3.3 Required optimization for a multifrequency system

The above-mentioned FSD technique is a differential measurement of the imaging signal obtained from the high-resolution frequency bands to construct the deviations from blackbody. Implementation of this method along with the standard imaging method (by using low resolution frequency bands) is required to achieve the science goals from the spectral distortions as well as the anisotropic part of CMB. So we need a hybrid composition of frequency resolution to implement both FSD technique and imaging technique, such that we can obtain the spectral distortion signal and anisotropic signal from the same conceptual framework and also with minimum cost and minimum error.

To minimize the sources of systematic error, it is required to reduce the contribution of CMB blackbody in the differential measurement between two different frequency channels. So we need high-resolution frequency channels to subtract the blackbody part substantially so that the total systematic error is smaller than the spectral distortion signal. The high-resolution FSD technique needs to be implemented on the frequency range that have the large values of FSD kernel for μ distortion (approximately 1−50 GHz) and y distortion (approximately 100−300 GHz), which can be identified from Fig. 3. The remaining frequency ranges can have large bandwidth to perform the scientific studies related to imaging. A detailed case study of the FSD technique can be done for a specific mission

with the knowledge of the detector properties, calibration error, data read-out frequency, size of the focal plane, etc.

For multiple frequency channels, we require to estimate the covariance matrix consisting of contributions from systematic errors[2] ($\mathbf{C}_{\rm sys}$), statistical error ($\mathbf{C}_N$), and error due to each cosmological and astrophysical component ($\mathbf{C}_A \equiv \langle \mathbf{A}\mathbf{A}^\dagger \rangle$). So the total covariance matrix becomes

$$\langle \mathcal{T}\mathcal{T}^\dagger \rangle \equiv \mathbf{C}_\mathcal{T} = \mathbf{D}\mathbf{C}_A\mathbf{D}^T + \mathbf{C}_{\rm sys} + \mathbf{C}_N. \tag{24}$$

The covariance matrix is not diagonal and needs to be evaluated for every mission with the particular instrumental noise, systematic errors and frequency coverage. The essential requirement to implement the FSD technique is to reduce the contribution of the total error on the signals of spectral distortion. The total contribution from the systematic and the instrumental noise matrix can be written as

$$\mathbf{C}_{\tilde{\mathcal{N}}} = \mathbf{C}_{\rm sys} + \mathbf{C}_N, \tag{25}$$

which can be decomposed as

$$\mathbf{C}_{\tilde{\mathcal{N}}} = \mathbf{E}\Gamma\mathbf{E}^T, \tag{26}$$

where $\mathbf{\Gamma}$ is a diagonal matrix of eigenvalues $\gamma_1, \gamma_2, \ldots, \gamma_n$ such that $\gamma_1 > \gamma_2 > \ldots > \gamma_n$ and the matrix $\mathbf{E}$ contains the corresponding eigenvectors. An experimental design that can achieve the condition that the eigenvectors with largest eigenvalues have a minimum projection on the FSD kernel (like D^μ_ν and D^y_ν for μ and y, respectively) can significantly improve the SNR of the measurement. In Section 4, we elaborate more on this and also explain the procedures to extract the signal.

3.4 Gain factor and the calibration error

For CMB experiments, there are several standard calibration sources (Planck Collaboration VIII 2016) like the CMB solar dipole, the orbital dipole, and planets. These are used for calibration by the *Planck* mission (Planck Collaboration VIII 2016). The orbital dipole is a very good calibrator due to the well-known value of the satellite velocity and gives a very small calibration error of typically $0.1 - 0.01$ per cent (Planck Collaboration VIII 2016). The motion of the solar barycentre (dipole) or the orbital motion (of the satellite) also exhibits a known spectrum that can be written as $\Delta T_{\rm dip} K^T_{\nu_i}$, where $\Delta T_{\rm dip}$ is the magnitude of the induced temperature due to the solar or the orbital motion and $K^T_{\nu_i}$ is the derivative of the blackbody spectrum with respect to the temperature. So using the known value of the brightness temperature of the CMB dipole and (time-dependent) orbital motion, we can calibrate the detectors for each frequency channel. For the remaining discussion in the paper we will focus only on the orbital dipole because of several factors like (i) ease of modelling accurately, (ii) measurement with very high SNR by current detectors, and (iii) clean demodulation from multiyear data due to its annual variation. Schematically, the CMB dipole can be measured within each frequency channel through its pixel-to-pixel variation

$$\delta S^{\rm dip}_{\nu_i} \equiv S_{\nu_i}(\hat{p}_1) - S_{\nu_i}(\hat{p}_2) = G_{\nu_i}(V_{\nu_i}(\hat{p}_1) - V_{\nu_i}(\hat{p}_2)) \equiv G_{\nu_i}\Delta V_{\nu_i}. \tag{27}$$

Due to the known frequency spectrum of $\delta S^{\rm dip}_{\nu_i}$, one can write this as

$$G_{\nu_i} = \frac{K^T_{\nu_i}\Delta T_{\rm dip}}{\Delta V_{\nu_i}}. \tag{28}$$

[2]Bold fonts denotes matrices.

As a result, the gain error in terms of the error associated with the dipole measurement ($\delta(\Delta T_{\rm dip})$) and voltage measurement ($\delta(\Delta V)$) can be written as

$$\left(\frac{\delta G_{\nu_i}}{G_{\nu_i}}\right)^2 \simeq \left(\frac{\delta(\Delta T_{\rm dip})}{\Delta T_{\rm dip}}\right)^2 + \left(\frac{\delta(\Delta V)}{\Delta V}\right)^2. \tag{29}$$

So the gain error of each channel is related to the error associated with the measurement of dipole amplitude, even if the error in the measurement of voltage is negligible.

We can accurately obtain the relative gain coefficients at different frequencies by cross-calibrating between frequency channels. By equating the dipole amplitude fluctuation $\Delta T_{\rm dip}$ between any two frequency channels, we can write

$$\frac{G_{\nu_j}\Delta V_{\nu_j}}{K^T_{\nu_j}} = \frac{G_{\nu_i}\Delta V_{\nu_i}}{K^T_{\nu_i}}, \tag{30}$$

which implies

$$\mathcal{G}_{ji} \equiv \frac{G_{\nu_j}}{G_{\nu_i}} = \frac{\Delta V_{\nu_i}}{\Delta V_{\nu_j}}\frac{K^T_{\nu_j}}{K^T_{\nu_i}}. \tag{31}$$

This indicates that the relative calibration depends only on the measured voltage difference. Therefore, the corresponding error in the ratio of the gain is affected only by the error associated with the measurement of voltage difference and not that associated with the orbital dipole measurement. As a result, the error on the relative gain ratio can be reduced. This also indicates that the accurate calibration of the gain factor at any one frequency channel translates into an accurate calibration at all channels. Though this step is not directly usable to calibrate the channels in the FSD method, it gives us an additional way to cross-calibrate different frequency channels. Systematic errors due to any additional sources can be regulated by comparing the relative outputs between the frequency channels.

4 SIGNAL EXTRACTION USING DIFFERENT TECHNIQUES

4.1 Fitting the FSD spectrum

The FSD measurement of the all-sky intensity (or equivalently brightness temperature) at different frequency channels is an addition of several signals due to cosmological and astrophysical sources and also instrumental noise. With the known spectrum of the FSD and a high spectral resolution measurement over a wide frequency band, we can estimate the best-fitting parameter $\hat{\mathcal{A}}_x$ (where $x \in [y,\ \mu, \ldots]$), which minimizes the chi-square defined as

$$\chi^2_{y\ ,\mu} = \sum_{\nu,\nu'}\left(\bar{\mathcal{T}}_\nu - \hat{\mathcal{A}}_{y,\mu}\mathcal{D}^{y,\mu}_\nu\right)(C^{-1}_\mathcal{T})_{\nu\nu'}\left(\bar{\mathcal{T}}_{\nu'} - \hat{\mathcal{A}}_{y,\mu}\mathcal{D}^{y,\mu}_{\nu'}\right). \tag{32}$$

Addition over a wide range of frequencies increases the overall SNR of the signal. The corresponding error bar on $\hat{\mathcal{A}}_{y,\mu}$ is a standard result given by

$$\sigma^2_{y,\mu} = \left[\sum_{\nu,\nu'}\mathbf{D}^{y,\mu}_\nu(\mathbf{C}^{-1}_\mathcal{T})_{\nu\nu'}\mathbf{D}^{y,\mu}_{\nu'}\right]^{-1}. \tag{33}$$

As mentioned before, the covariance matrix $\mathbf{C}_\mathcal{T}$ is non-diagonal and is a quantity that depends upon instrumental noise, scanning strategy, systematic errors, etc. For a particular mission, these quantities need to be evaluated for successfully implementing the FSD technique.

4.2 Internal linear combination method

After the removal of the coupling between gain errors and the CMB monopole the main remaining hurdle to measuring μ and y distortions is foreground contamination. At low frequencies, the main sources of contamination are synchrotron emission and spinning dust emission from our galaxy. At high frequency, foreground contamination is mainly due to dust. Since the FSD spectrum of μ and y are not degenerate with these foregrounds, we will now discuss how to use combinations of frequency channels over a wide range of frequencies to project out foreground contamination.

We at first address the extraction of the monopole part of the spectral distortion signal by an all-sky average of the FSD spectrum. The all-sky average value of the distortion signal can be extracted using the known FSD spectrum (equation 8) by the internal linear combination (ILC; Remazeilles, Delabrouille & Cardoso 2011) and modified internal linear combination algorithm (MILCA; Hurier et al. 2013). With M_ν frequency channels over which $\mathcal{T}_i$ is estimated, we can write

$$\mathcal{T}_{\nu_i} \equiv \mathcal{T}_{\nu_i}(\hat{p}) = \mathcal{D}^j_{\nu_i} \Delta\nu_i A^j(\hat{p}) + N_{\nu_i}(\hat{p}), \tag{34}$$

where $i \in [1, M_\nu]$ and $A^j \equiv [A_{CMB}, A_\mu, A_y, \ldots, A_{N_s-1}]$. A^j contains both cosmological signal and also foreground contaminations. In terms of the $M_\nu \times 1$ column vector $\mathcal{T}$, $N_s \times 1$ column vector $\boldsymbol{A}$ and $M_\nu \times N_s$ mixing kernel $\mathbf{D}$, we can write

$$\mathcal{T} = \mathbf{DA} + \mathbf{N}. \tag{35}$$

In the presence of a non-zero value of ΔG (introduced in the previous section), there is also an additional component given by

$$\mathcal{T}_{\nu_i} = \mathcal{D}^j_{\nu_i} \Delta\nu_i A^j(\hat{p}) + N_{\nu_i}(\hat{p}) + \tfrac{\Delta G_{\nu_i}}{G_{\nu_i}} \mathcal{S}^{\rm pl}_{\nu_i}, \tag{36}$$

$$\mathcal{T} = \mathbf{DA} + \mathbf{N} + \mathbf{J}_G, \tag{37}$$

where $\mathcal{S}^{\rm pl}_{\nu_i}$ is the FSD blackbody spectrum at frequency ν_i and $\mathbf{J}_G$ is the residual column matrix that can arise due to difference in the gain of the frequency channels. The extraction of the signal is achievable with the requirement that we recover only one component and follow the constraint that all other components do not contribute to the signal. For N_s rejected components, we can define weights $\boldsymbol{w}$ such that

$$\begin{aligned}
u_1 &= \boldsymbol{w}^T \boldsymbol{f_1} = 0,\\
u_2 &= \boldsymbol{w}^T \boldsymbol{f_2} = 0,\\
&\vdots \qquad\quad \vdots\\
u_j &= \boldsymbol{w}^T \boldsymbol{f_j} = 1,\\
&\vdots \qquad\quad \vdots\\
u_{N_s} &= \boldsymbol{w}^T \boldsymbol{f}_{N_s} = 0,\\
u_{N_s+1} &= \boldsymbol{w}^T \mathbf{J}_G = 0,
\end{aligned} \tag{38}$$

where $\boldsymbol{f}_j$ are the frequency dependence of the jth signal defined as $\boldsymbol{f_j} = \boldsymbol{\mathcal{D}x_j}$. $\boldsymbol{f}_j$ is a column vector with $M_\nu \times 1$ elements and $\boldsymbol{x_j} = [0, 0, \ldots, 1, \ldots, 0]^T$ with only jth element equal to one. The last condition of equation (38) also put constraints on the nature of relative gain difference $\Delta G_i/G_i$. For the FSD technique to work, $\mathbf{J}_G$ should not behave like any of the spectral signatures like μ, y, etc. and hence needs to satisfy the condition

$$\left[\mathbf{J}_G \boldsymbol{f}_j\right]_i = \frac{\Delta G_{\nu_i}}{G_{\nu_i}} \mathcal{S}^{\rm pl}_{\nu_i} f^j_{\nu_i} = 0. \tag{39}$$

As $S^{\rm pl}_{\nu_i}$ is the known FSD spectrum of blackbody at frequency ν_i, so the required frequency dependence of $\Delta G_{\nu_i}/G_{\nu_i}$ to minimize the residual contaminations in the signal is manifested by equation (39). By combining the measurement of $\Delta G_{\nu_i}/G_{\nu_i}$ from different frequency channels, we can infer any projection of the gain error on the spectral distortion signals and hence will subtract it prior to the calibration of the FSD signals. A special case with $\Delta G_{\nu_i} = 0$ is a trivial solution of this equation and is sufficient but not necessary to be satisfied by the detectors. In the remaining of the paper, we will assume that the correction from $\Delta G_{\nu_i}/G_{\nu_i}$ can be made and we restrict only to N_s values of u.

With the requirement that the variance in the extracted *signal* map $\mathbf{C}_{\hat{\mathcal{A}}} = \langle \hat{A}\hat{A}^T \rangle$ is minimum, the weight matrix can be obtained by solving the equation

$$\begin{bmatrix} 2\mathbf{C}_\mathcal{T} & -\mathbf{D} \\ \mathbf{D}^T & 0 \end{bmatrix} \begin{bmatrix} \boldsymbol{w} \\ \lambda \end{bmatrix} = \begin{bmatrix} 0 \\ \boldsymbol{x} \end{bmatrix}, \tag{40}$$

where λ is the Lagrange multiplier and the covariance matrix $\mathbf{C}_\mathcal{T}$ is a $\mathbf{M}_\nu \times \mathbf{M}_\nu$ dimension matrix that can be expressed as

$$\mathbf{C}_\mathcal{T} = \mathbf{D}^T \mathbf{C_A} \mathbf{D} + \mathbf{C}_{\tilde{\mathbf{N}}}, \tag{41}$$

where $\mathbf{C}_{\tilde{\mathbf{N}}}$ is defined in equation (25) and have the contributions from instrumental noise, systematic errors, and covariance matrix of the cosmological and astrophysical sources.

The weight matrix that satisfies equation (40) can be expressed as

$$\mathbf{W} = \mathbf{C}^{-1}_\mathcal{T} \mathbf{D} (\mathbf{D}^T \mathbf{C}^{-1}_\mathcal{T} \mathbf{D})^{-1}, \tag{42}$$

and the corresponding jth component of the map can be obtained as

$$\hat{\mathcal{A}}_j = \boldsymbol{x}^T_j \mathbf{W}^T \mathcal{T}. \tag{43}$$

The error estimate of the signal map $\hat{\mathcal{R}}_j$ can be written as

$$\mathbf{C}_{\hat{\mathcal{A}}_j} = \boldsymbol{x}^T_j \mathbf{W}^T \mathbf{C}_\mathcal{T} \mathbf{W} \boldsymbol{x}_j. \tag{44}$$

Using the above formalism for every component of the signal, we can obtain the weight matrix $\mathbf{W}$ that minimizes the variance of the signal. To further reduce the error of the signal, we can satisfy the condition similar to equation (26) for the covariance matrix $\mathbf{C}_\mathcal{T}$ such that weight matrix projects minimally with the eigenvector corresponding to the largest eigenvalue of the covariance matrix. So the error estimate on the jth component in terms of the eigenvector decomposition ($\mathbf{C}_\mathcal{T} = \mathbf{E}_\mathcal{T} \Gamma_\mathcal{T} \mathbf{E}_\mathcal{T}{}^{-1}$) can be written as

$$\mathbf{C}_{\hat{\mathcal{A}}_j} = \boldsymbol{x}^T_j \mathbf{W}^T \mathbf{E}_\mathcal{T} \Gamma_\mathcal{T} \mathbf{E}_\mathcal{T}{}^{-1} \mathbf{W} \boldsymbol{x}_j, \tag{45}$$

which satisfies the condition

$$\boldsymbol{x}^T_j \mathbf{W}^T \mathbf{E}^i_\mathcal{T} \approx 0 \;\forall\, \gamma_i > \gamma_{\rm min}. \tag{46}$$

where $\gamma_{\rm min}$ is the smallest eigenvalue of the covariance matrix $\mathbf{C}_\mathcal{T}$.

4.3 Measurement of spatial variations in the spectral distortion

The methods described previously have a particular application for approaching the monopole part of the spectral distortion signal. However, this approach can be readily extendable to measure the fluctuations in the spectral distortion signal. Measurement of the FSD signal at every frequency channel gives a pixel space map of the signal, which in general can be written as

$$\mathcal{T}_{\nu_i}(\hat{p}) = \textstyle\sum_j D^j_{\nu_i} \Delta\nu_i A^j(\hat{p}), \tag{47}$$

$$(\mathcal{T}_{\nu_i})_{lm} = \textstyle\sum_{lm} \sum_j D^j_{\nu_i} \Delta\nu_i (A^j)_{lm}, \tag{48}$$

where $(\mathcal{T}_{\nu_i})_{lm}$ and $(A^j)_{lm}$ are the spherical harmonics transformation of $\mathcal{T}_{\nu_i}(\hat{p})$ and $A^j(\hat{p})$, respectively. The fluctuations in the signal can be captured by the power spectrum ${}_{\nu}C_l^{\mathcal{T}\mathcal{T}} = \frac{\sum_m (\mathcal{T}_\nu)_{lm}(\mathcal{T}_\nu^*)_{lm}}{(2l+1)}$ that is a composite effect of all the mechanisms. The dominant source of fluctuations in the spectral distortion is due to the y distortion (Hill et al. 2015). With this technique, we can access the spatial fluctuations in the spectral distortions that are expected to be stronger than μ distortions. The intrinsic temperature fluctuations exhibit a very different FSD spectrum from y and hence are easily separable. The ILC method for FSD signal discussed previously is also directly applicable to reconstructing the signal at every pixel and to generating a map of the fluctuations.

5 REQUIREMENTS TO USE FSD

While not using an absolute internal calibrator to measure CMB spectral distortions has clear practical advantages, the both approaches have their unique features and challenges. For an absolute internal calibrator, it is essential that the calibrator is stable in temperature and is a perfect blackbody so that it matches the blackbody distribution of CMB. Even a tiny departure from the blackbody spectrum of the absolute internal calibrator can act as a source of systematic error and obscure any cosmological spectral distortion. In the absence of an absolute internal calibrator, we have to achieve good control of the systematic errors in the temperature measurement and excellent relative calibration of different frequency channels, but for a potentially significant reduction in mission complexity and hence cost.

We now discuss the necessary requirements to use FSD for detecting CMB spectral distortions.

(i) Instrument and measurement technique should be designed such that the final output is calibrated only with the relative voltage difference between two frequency channels as discussed in Section 3.2.

(ii) The FSD signal due to y and μ distortions peak at different frequency ranges as shown in Fig. 3. So, multiple high spectral resolution channels in those frequency range should be implemented with minimum instrumental noise. Use of high spectral resolution channels can help in reducing the contaminations from other sources and also improve the systematic errors in the measurement.

(iii) Measurement techniques should be devised such that the coupling of the FSD spectrum of the signal with the eigenvectors corresponding to the largest eigenvalues of the noise covariance matrix is minimized. This can improve the measurability of the spectral distortion signal and reduce the contamination from systematic error and instrumental noise.

(iv) The relative difference in the gain factor G between frequency channels should satisfy the condition given in equation (39).

(v) A stable gain factor G for the complete frequency range is required with a very small relative calibration error of $\delta G/G$ between different frequencies. The requirement for a controlled gain error is provided in Section 3.4.

(vi) The systematic errors due to off-set temperature of the detectors must be controlled below the desired signal S_ν^μ and S_ν^y at every frequency channel.

6 STEPS TO IMPLEMENT FSD METHOD

In this section, we briefly elaborate the steps one needs to perform in order to implement the FSD method by using orbital/solar dipole as a calibrator. Though the exact calibration method will depend on the details of the detector technology, frequency channels, and instrument properties, we summarize here the sequential steps one should follow to implement this method. For this discussion, we assume that the output is measured as the power incident on the detectors. This method is also applicable for an antenna like set-up.

The bolometer-like detectors measure the total power at a particular frequency and gives output in terms of the voltages. The measured voltage at a particular frequency ν and sky direction $\hat{p}$ is related to the sky temperature by the relation equation (13)

$$S_{\nu_i}(\hat{p}) = G_{\nu_i} V_{\nu_i}(\hat{p}) + T_{\nu_i}^{\rm off}, \tag{49}$$

A differential measurement between two directions but at same frequency gives us

$$S_{\nu_i}(\hat{p}_1) - S_{\nu_i}(\hat{p}_2) = G_{\nu_i}(V_{\nu_i}(\hat{p}_2) - V_{\nu_i}(\hat{p}_1)). \tag{50}$$

For a known orbital/solar dipole measurement of $S_{\nu_i}(\hat{p}_1) - S_{\nu_i}(\hat{p}_2)$, we can calibrate the voltage difference as mentioned in equation (27). This induces an error δG_{ν_i} as mentioned in equation (29).

The calibration of the all sky average brightness temperature (which relates to the blackbody temperature of CMB) can be calibrated using these gain factors with an error

$$\delta S_{\nu_i}^{\rm pl} = \frac{\delta G_{\nu_i}}{G_{\nu_i}} S_{\nu_i}^{\rm pl}. \tag{51}$$

So for $T_{\nu_i} = 2.7255$ K, the error in δT_{ν_i} in K is of the same order of the gain error.

For the FSD method, we propose to measure the difference of the output voltage between two frequency channels, $\Delta V_{ij} = V_{\nu_i} - V_{\nu_j}$. Then we convert this quantity into the difference in the sky temperature between two frequency channels using equation (20). The corresponding measurement error in the FSD signal can be calculated using equation (21). For the FSD case, the error is related to the difference in the sky brightness temperature between two frequency channels and not with the value of brightness temperature itself, i.e.

$$(\delta\mathcal{T}_{\nu_{ij}})^2 = \left[\left(\frac{\delta G_{\nu_i}}{G_{\nu_i}}\right)^2 + \left(\frac{\delta G_{\nu_j}}{G_{\nu_j}}\right)^2\right]\left(\mathcal{S}_{\nu_{ij}}\right)^2. \tag{52}$$

As the difference between the sky temperature between two frequency channels ($\mathcal{S}_{\nu_{ij}}$) nearly vanishes for the blackbody distribution, the induced variance $(\delta\mathcal{T}_{\nu_{ij}})^2$ in the measurement of the signal is also reduced in comparison to the case when there is an absolute measurement, as mentioned in equation (51).

The crucial difference in calibrating the absolute temperature value and FSD temperature spectrum is the reduction in the systematic error as can be seen in equations (51) and (52). Equation (51) couples with $S_{\nu_i}^{\rm pl} \approx 2.7255$ K in RJ limit, whereas equation (52) couples with $\mathcal{S}_{\nu_{ij}}$ which is of the order of 10^{-2} K in the RJ limit and for unit frequency band width ($\Delta\nu = 1$ GHz). FSD is not the difference of the already calibrated absolute sky temperature. It is the measurement of difference in the voltages from the detectors working at two different frequency channels and then converting the voltage difference into the corresponding FSD sky temperature.

Steps for the implementation of FSD method:

(i) Calibrate the gain factor G_ν at each frequency channel using the orbital/solar dipole. This gives a set of values of gain as $[G_{\nu_1}, G_{\nu_2}, G_{\nu_3}, \ldots, G_{\nu_n}]$ for n frequency channels. From this, we can also obtain the difference in the mean value of gain factor between different pairs of channels like $\Delta G_{\nu_{ij}} = G_{\nu_i} - G_{\nu_j}$.

(ii) The measurement of ΔG_ν assures the implementation of equation (39). As long as the difference in the gain factors do

not mimic any spectral distortion spectrum like y, μ, etc., we can satisfy the requirement of equation (39). So, the array of difference in the gain factor, $\boldsymbol{J_G}$, can be obtained by this method.

(iii) The FSD detector set-up is arranged such that it can estimate only the difference in voltages between two frequency channels of the bolometers (or the corresponding output for other kinds of detectors), and multiply it with the gain factor to get the FSD sky temperature as shown in equation (17).

(iv) With the FSD sky temperature measurement and the mean differences in the gain factor between different frequency channels $\boldsymbol{J_G}$, we can implement the method mentioned in Section 4 to extract the spectral distortion signal.

7 CONCLUSIONS

The rich domain of cosmological information embedded in the spectral distortion of the CMB spectrum is going to be unveiled by the next generation of CMB missions. The CMB absolute intensity is usually compared with an internal blackbody calibrator to search for any deviations from blackbody. In the presence of an internal blackbody calibrator, the observed intensity of the sky is compared at every frequency with the intensity from the internal blackbody calibrator and any departure of the observed sky intensity from the blackbody can be modelled with the known spectrum of spectral distortions. As a result, a successful measurement of spectral distortion signals with a high SNR requires the internal blackbody calibrator to be extremely stable at a fixed temperature and also should obey a perfect blackbody spectrum over the complete frequency range of a mission (typically 1−1000 GHz). The departure of the internal calibrator from blackbody can induce a systematic error and can also be misunderstood with the spectral distortion signal.

We propose an alternative strategy called the FSD to measure spectral distortions in CMB. This technique measures the difference in the observed brightness temperature at different frequencies and models the observed difference with the theoretically predictable FSD kernel for different components in equation (8). The FSD spectrum for expected sources of spectral distortions like μ and y are different and not degenerate, which makes it easily distinguishable and extractable. The μ spectrum is stronger at low frequencies and decreases rapidly at higher frequencies, whereas y distortion FSD spectrum is dominant at high frequency range as depicted in Fig. 3.

Our proposed method uses the CMB itself between the neighbouring channels as a calibrator to measure the deviations from blackbody. This method does not directly measure the absolute blackbody spectrum, but only measures the FSD of a blackbody signal. In the presence of spectral distortions, the FSD signal exhibits a combination of effects from blackbody along with other sources and can be fitted uniquely for a known FSD spectrum. Successful implementation of the FSD method needs several instrumental controls in order to reduce contaminations by systematic errors and instrumental noise, which we listed in Section 5. Measurement of the spectral distortion signal without an internal absolute blackbody calibrator can be possible in implementing this formalism via suitable instrumental engineering for future missions.

The main insight of this paper is to explore signatures of spectral distortion and measuring any deviations from blackbody through the FSD spectrum. This process enables one to measure the spectral distortion signal in the same spirit as *WMAP* measured the CMB anisotropies through a differential measurement without an internal reference. The main advantage of our method is that it does not require an internal blackbody calibrator to measure the signal. Secondly, this approach opens up an alternative way of measuring the spectral distortion signal that can be useful for comparing results from other missions that use an internal blackbody calibration method. Next-generation CMB missions with upgraded detector technologies can implement this method to measure spectral distortions without using an absolute calibrator. Estimation of the noise properties and experimental requirements in order to implement this method for a future CMB mission like LiteBIRD (Matsumura et al. 2016) will be addressed in a follow-up paper.

ACKNOWLEDGEMENTS

This work has been done within the Labex ILP (reference ANR-10-LABX-63) part of the Idex SUPER, and received financial state aid managed by the Agence Nationale de la Recherche, as part of the programme Investissements d'avenir under the reference ANR-11-IDEX-0004-02. The work of JS has been supported in part by ERC Project No. 267117 (DARK) hosted by the Pierre and Marie Curie University-Paris VI, Sorbonne Universities. The work of SM and BDW is supported by the Simons Foundation. The authors acknowledge valuable comments from Masashi Hazumi on this draft. Authors thank Eiichiro Komatsu for valuable discussions and comments on this work.

REFERENCES

André P. et al., 2014, JCAP, 1402, 006
Balashev S. A., Kholupenko E. E., Chluba J., Ivanchik A. V., Varshalovich D. A., 2015, ApJ, 810, 131
Bleem L. E. et al., 2015, ApJS, 216, 27
Chluba J., 2010, MNRAS, 402, 1195
Chluba J., 2016, MNRAS, 460, 227
Chluba J., Sunyaev R. A., 2012a, MNRAS, 419, 1294
Chluba J., Sunyaev R. A., 2012b, MNRAS, 419, 1294
Chluba J., Khatri R., Sunyaev R. A., 2012, MNRAS, 425, 1129
Dunkley J. et al., 2009 , in AIP Conf. Proc. Vol. 1141, CMB Polarization Workshop: Theory and Foregrounds. Am. Inst. Phys., New York, p. 222
Emami R., Dimastrogiovanni E., Chluba J., Kamionkowski M., 2015, Phys. Rev., D91, 123531
Fixsen D. J., 2009, ApJ, 707, 916
Fixsen D. J., Hinshaw G., Bennett C. L., Mather J. C., 1997, ApJ, 486, 623
Hasselfield M. et al., 2013, JCAP, 1307, 008
Hill J. C., Battaglia N., Chluba J., Ferraro S., Schaan E., Spergel D. N., 2015, Phys. Rev. Lett., 115, 261301
Hu W., Scott D., Silk J., 1994, ApJ, 430, L5
Hurier G., Macías-Pérez J. F., Hildebrandt S., 2013, A&A, 558, A118
Khatri R., Sunyaev R. A., 2012a, JCAP, 1206, 038
Khatri R., Sunyaev R. A., 2012b, JCAP, 1209, 016
Khatri R., Sunyaev R., 2015a, JCAP, 1508, 013
Khatri R., Sunyaev R., 2015b, JCAP, 1509, 026
Khatri R., Sunyaev R. A., Chluba J., 2012, A&A, 543, A136
Kholupenko E. E., Balashev S. A., Ivanchik A. V., Varshalovich D. A., 2015, MNRAS, 446, 3593
Kogut A. et al., 2011, JCAP, 7, 025
Mather J. C. et al., 1994, ApJ, 420, 439
Mather J. C., Fixsen D. J., Shafer R. A., Mosier C., Wilkinson D. T., 1999, ApJ, 512, 511
Matsumura T. et al., 2016, J. Low. Temp. Phys., 184, 824
Pajer E., Zaldarriaga M., 2012, Phys. Rev. Lett., 109, 021302
Planck Collaboration VIII, 2016, A&A, 594, A8
Planck Collaboration X, 2016, A&A, 594, A10
Planck Collaboration XXVII, 2016, A&A, 594, A27
Remazeilles M., Delabrouille J., Cardoso J.-F., 2011, MNRAS, 410, 2481

Richards P. L., 1994, J. Appl. Phys., 76, 1
Sathyanarayana Rao M., Subrahmanyan R., Udaya Shankar N., Chluba J., 2015, ApJ, 810, 3
Sironi G., 2017, JCAP, 1702, 023
Smoot G. F. et al., 1991, ApJ, 371, L1
Staniszewski Z. et al., 2009, ApJ, 701, 32
Sunyaev R. A., Chluba J., 2009, Astron. Nachr., 330, 657
Sunyaev R. A., Zeldovich Y. B., 1970, Ap&SS, 9, 368
Zeldovich Y. B., Sunyaev R. A., 1969, Ap&SS, 4, 301

This paper has been typeset from a TEX/LATEX file prepared by the author.